NEXIALOG
CONSULTING

FINANCIAL SCENARIO MODELING

UNDER TRANSITION UNCERTAINTY

SEPTEMBRE 2026

Financial Scenario Modeling Under Transition Uncertainty

Baye Matar Kandji Anthony Pierre

Septembre 2026

Abstract

Integrating climate transition risks into long-term asset-liability management has become a strategic priority for the insurance industry. Beyond regulatory compliance, developing resilient Strategic Asset Allocation and the viability of multi-year Strategic Business Plans require modeling frameworks that integrate structural changes related to the energy transition. Economic Scenario Generators (ESGs) provide the analytical foundation for these projection exercises. However, conventional ESGs, calibrated on historical data, fail to capture the structural breaks induced by the energy transition. Moreover, the central trajectories published by the Network for Greening the Financial System (NGFS), while widely used as transition narratives, ignore both the dispersion around their baseline trajectories and the uncertainty about which pathway is actually unfolding. To address these limitations, this paper proposes a unified modeling framework that extends the benchmark Ahlgrim ESG model. We integrate forward-looking transition risks by linking future financial and macroeconomic dynamics directly to these climate scenarios, while using Bayesian filtering to quantify the underlying scenario uncertainty.

Keywords: Economic scenario generator, climate transition risk, NGFS scenarios, Ahlgrim model, Solvency II, Bayesian filtering.

32 Rue de Trévise, 75009 Paris, France.
Nexialog Consulting

1 Introduction

Climate change represents a systemic risk to global financial stability. Its financial transmission channels divide into physical risks, driven by extreme weather events and long-term climatic shifts, and transition risks, arising from the technological, regulatory, and economic adjustments required to reach a net-zero economy (Battiston et al., 2017; NGFS, 2019). These risks affect insurers on both sides of their balance sheet: physical risks weigh on property and casualty underwriting, in particular natural-catastrophe coverage, and can alter mortality rates in life insurance, while the transition risks threatens long-term investment portfolios through the devaluation of stranded assets. Embedding these structural risks into asset-liability management (ALM) and solvency frameworks has therefore become a regulatory and operational necessity.

The exploratory stress tests conducted by prudential authorities and central banks between 2021 and 2025, including the ACPR's pilot exercises (ACPR, 2021, 2024) and the ECB's climate stress test (ECB, 2022), have provided initial quantifications of these impacts. For instance, the ACPR's 2024 climate stress test, covering 90% of the French insurance market, showed that transition shocks could reduce aggregate Solvency Capital Requirement coverage ratios from 230% to 170% under adverse conditions. Building on these findings, the revised Solvency II framework (Directive (EU) 2025/2), with which compliance is required by January 2027, mandates the inclusion of at least two long-term climate scenarios in the ORSA, one consistent with a 2°C warming limit and one significantly above it. Beyond regulatory compliance, developing resilient Strategic Asset Allocation (SAA) and ensuring Strategic Business Plans (SBP) viability require modeling frameworks that integrate structural changes related to the energy transition. To meet these requirements, insurers rely on Economic Scenario Generators (ESGs). The ESG model of Ahlgrim et al. (2005) model remains the standard reference for insurance applications. It connects inflation, real interest rates, equity returns, dividend yields, and real estate within a coherent cascade.

There is a common methodological limitation among traditional ESG models: they rely exclusively on historical calibration. This approach assumes that long-term macroeconomic dynamics are stationary, which is incompatible with climate transition trajectories that project lasting shifts in inflation, interest rates, and asset returns as carbon pricing takes effect (Vermeulen et al., 2021; Allen et al., 2020). Furthermore, Trust et al. (2023) show that models blind to such structural breaks produce loss estimates that are too optimistic and Boudreault et al. (2023) note that climate change invalidates the actuarial approach of extrapolating the past.

The macroeconomic scenarios published by the NGFS (NGFS, 2020, 2023, 2024a) partially address this gap. They rely on integrated assessment models (IAMs) such as REMIND, MESSAGEix-GLOBIOM, and GCAM to project macro-financial variables across orderly, disorderly, and hot-house pathways. However, these trajectories are deterministic by construction and capture neither the dispersion of plausible paths around each baseline nor the uncertainty about which scenario is actually unfolding. A growing literature formalizes scenario uncertainty through Bayesian learning. Flora and Tankov (2023) show that the dynamic inference of climate regimes from observable signals such as carbon emissions is a material risk factor, reducing the valuation of green and brown investments by 7% and 25%, respectively, relative to a perfect-foresight environment. Mazzon and Tankov (2024) extend this approach to Knightian ambiguity, and Chekriy et al. (2025) apply Bayesian learning to track corporate decarbonization, introducing a "Budget-at-Risk" metric that quantifies the probability of a firm exceeding its cumulative carbon budget under scenario uncertainty. Dione (2025) extract a latent climate factor from NGFS trajectories using principal component analysis embedded in a neural network.

To address these limitations, this paper proposes such an extension of the Ahlgrim model. The contribution is twofold. First, we develop a modeling framework in which future trends align with climate scenario dynamics. Second, we formalize transition scenario uncertainty through a discrete latent variable, inferred recursively via a Hamilton filter driven by an observable decarbonization signal. The model integrates regime-conditioned trajectories for inflation, interest rates, equities, and real estate. The estimation process consists of two stages. First, classical univariate techniques are applied to historical volatility parameters. Then, an Expectation-Maximization (EM) algorithm is applied to calibrate the latent climate factor dynamics, refine the volatility calibration, and incorporate scenario uncertainty into calibrated parameters using scenario data.

The remainder of the paper is organized as follows. Section 2 presents the NGFS climate scenarios used as structural inputs. Section 3 discusses the Ahlgrim model and its climate extension. Section 4 describes the two-stage calibration process. Section 5 applies the framework to portfolio allocation under climate uncertainty and the Appendices contain technical derivations.

2 Climate scenarios

Climate scenarios provide a structured methodology for projecting the combined effects of climatic shifts, public policy responses, and macroeconomic outcomes. Initially designed to guide policy formulation, they have become the standard for prudential stress testing in the banking and insurance sectors. Under the revised Solvency II framework, their integration into the ORSA is a compliance requirement.

Several organizations, including the IPCC, the IEA, the ECB, and the Network for Greening the Financial System (NGFS), publish climate scenarios. Among these, the NGFS framework has become the standard for macroeconomic risk assessment. NGFS scenarios are produced by Integrated Assessment Models (IAMs), such as REMIND-

MAgPIE (Baumstark et al., 2021), MESSAGEix-GLOBIOM (Huppmann et al., 2019), and GCAM (Calvin et al., 2019). The outputs are then converted into macroeconomic variables, including GDP, inflation, interest rates, and housing indices, using the National Institute Global Econometric Model (NiGEM) developed by the NIESR.

The NGFS architecture organizes pathways by the timing, coordination, and stringency of climate policy. Orderly scenarios assume immediate, coordinated implementation: *Net Zero 2050* limits warming to 1.5°C and reaches carbon neutrality by mid-century, *Below 2°C* maintains warming below 2°C with 67% probability through more gradual policy intensification, and the *Low Demand* variant adds structural reductions in energy consumption. Disorderly scenarios model delayed or fragmented responses: under *Delayed Transition*, no new measures are enacted before 2030 and an abrupt policy shock follows, while *Fragmented World* captures heterogeneous regional policies and maximizes both transition costs and physical damages. Hot-house scenarios assume policy failure: *Nationally Determined Contributions* limit action to existing Paris pledges, and *Current Policies* adds no further measures, leading to warming approaching 3°C.

Our numerical application is based on the four highly distinct, representative NGFS scenarios: *Net Zero 2050*, *Delayed Transition*, *NDCs*, and *Current Policies*.

Figures 1a, 1b, 1c, and 1d respectively illustrate NGFS scenario dynamics for European Union GHG emissions and French macroeconomic indicators: inflation, long-term interest rates, and residential real estate index prices.

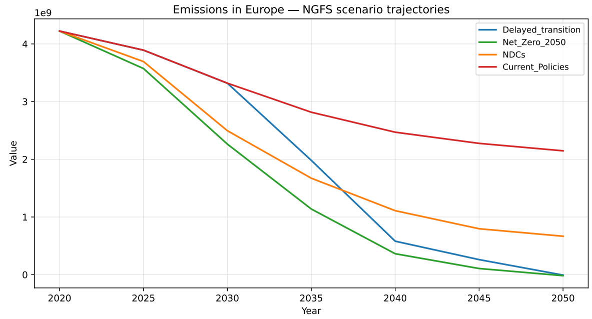

(a) GHG emissions

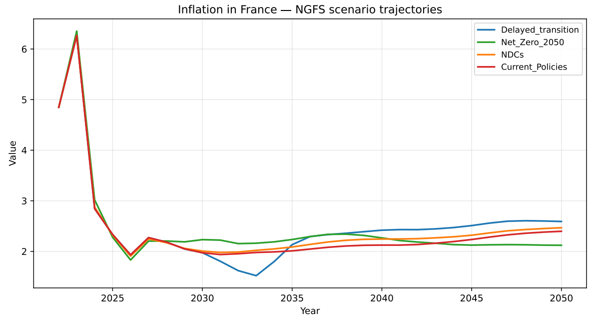

(b) Inflation rate

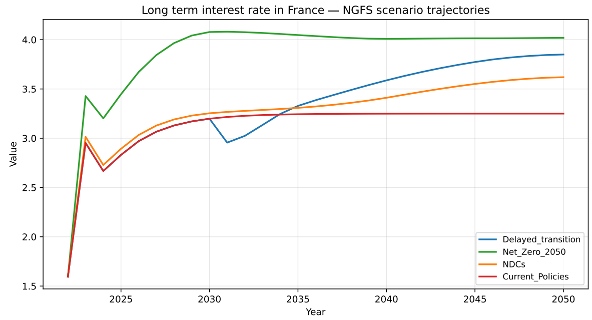

(c) Long-term interest rate

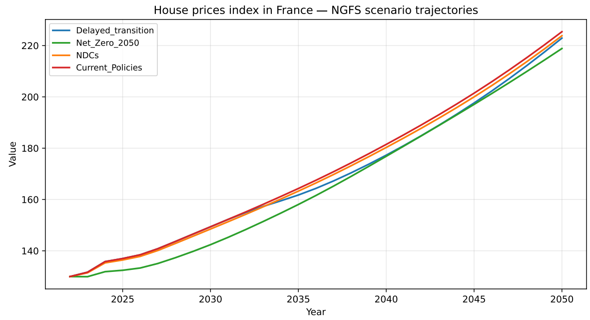

(d) Residential real estate index price

Figure 1: Historical and projected trajectories of macroeconomic and environmental variables under NGFS scenarios.

3 Model specification

This section develops the climate extension of the Ahlgrim model. We first recall the original specification, then describe the extension and the filtering problem induced by the latent scenario variable.

3.1 The Ahlgrim model

The model of Ahlgrim et al. (2005), developed under a joint initiative of the Casualty Actuarial Society (CAS) and the Society of Actuaries (SOA), generates stochastic economic scenarios by integrating interdependent financial variables. Following the approach of Wilkie (1986), the Ahlgrim model uses inflation as the driving variable. Let q_t, r_t, l_t, s_t, y_t, and m_t denote, respectively, the inflation rate, the short-term real interest rate, the long-term real interest rate, the equity return, the dividend yield, and the real estate return at time t.

Inflation, dividends, and real estate are modeled as Ornstein-Uhlenbeck (OU) processes:

$$dz_t = \kappa_z(\mu_z - z_t)\,dt + \sigma_z\,dW_{z,t}, \tag{1}$$

where z_t denotes, as appropriate, the inflation rate q_t, the real estate return m_t, or the log-dividend yield y_t. The parameters $\kappa_z > 0$, μ_z, and $\sigma_z > 0$ represent the speed of mean reversion, the long-run mean, and the volatility, respectively.

Real interest rates follow a two-factor Vasicek model, in which the short rate r_t is driven by the long rate l_t:

$$\begin{cases} dr_t = \kappa_r(l_t - r_t)\,dt + \sigma_r\,dW_{r,t}, \\ dl_t = \kappa_l(\mu_r - l_t)\,dt + \sigma_l\,dW_{l,t}. \end{cases} \tag{2}$$

Regarding equity returns, the log-return on equities (excluding dividends) decomposes into the sum of the nominal short rate and a risk premium:

$$ds_t = (q_t + r_t)\,dt + dx_t, \tag{3}$$

where the risk premium process $\{x_t\}$ follows the regime-switching model of Hardy (2001):

$$dx_t|\ \rho_t = \mu^{(x)}_{\rho_t}\,dt + \sigma^{(x)}_{\rho_t}\,dW^{(x)}_t, \quad \text{with} \quad p_{ij} = \mathbb{P}\big[\rho_{t+\delta} = j \mid \rho_t = i\big], \quad i, j \in \{1, \dots, d\}. \tag{4}$$

The Ahlgrim model represents a major advance in integrated actuarial modeling. Its coherent cascade structure and decomposition into analytically tractable processes make it well-suited to dynamic financial analysis, solvency margin assessment, and capital allocation exercises. However, the stationarity assumption implied by a fixed set of parameters, particularly the long-run means μ_z, is a significant limitation. Furthermore, because the model relies on historical data calibration, it fails to incorporate forward-looking economic expectations regarding transition risks, a shortcoming noted by Boudreault et al. (2023).

3.2 Climate extension of the model

We propose an extension of the Ahlgrim model that pursues two objectives: integrating the forward-looking trends from climate scenarios into risk factor dynamics, and modeling uncertainty about which transition scenario is actually in effect.

3.2.1 Latent scenario variable

We assume the existence of k possible climate scenarios, represented by a discrete latent variable $\Delta_t \in \{1, \dots, k\}$, for all t, following a Markov chain with transition matrix P and initial distribution π. The climate scenario is not directly observable; the economic agent perceives only signals from which the prevailing regime can be inferred.

3.2.2 Decarbonization signal

In the spirit of Ahlgrim et al., who introduce the unemployment rate as an auxiliary variable to improve risk factor forecasting, we propose a process describing the aggregate economic decarbonization rate c_t. This process exhibits a strong correlation with the transition state Δ_t and provides a natural signal for filtering the underlying scenario. The information set available at time t is defined by the σ-algebra:

$$I_t = \sigma\big(\Delta_{s+1},\, c_s,\, q_s,\, r_s,\, S_s,\, y_s,\, m_s \mid s \le t\big).$$

The variable Δ_t is therefore measurable with respect to I_{t-1}.

3.2.3 Risk factor dynamics

The proposed extensions replace the constant long-run means of the Ahlgrim model with time-varying means conditioned on the prevailing climate scenario, using a Hull-White specification.

Inflation and the decarbonization process follow respectively a Hull–White dynamic and an arithmetic Brownian motion with time-varying drift:

$$dz_t \mid \Delta_t = \mathbb{1}_{\{\kappa^{(z)}=0\}}\, \mu^{(z)}_{t,\Delta_t}\, dt + \kappa^{(z)}\big(\mu^{(z)}_{t,\Delta_t} - z_t\big)\, dt + \sigma^{(z)}\, dW^{(z)}_t, \tag{5}$$

where $z_t \in \{c_t, q_t\}$, $\mu^{(z)}_{t,\Delta_t}$ denotes the scenario-conditioned level, $\sigma^{(z)}$ is the volatility, and $\kappa^{(z)} \ge 0$ is the mean-reversion speed. When $\kappa^{(z)} > 0$, one recovers the standard Hull–White specification; when $\kappa^{(z)} = 0$, the process reduces to an arithmetic Brownian motion with time-varying drift $\mu^{(z)}_{t,\Delta_t}$.

For notational convenience, we introduce the *effective drift coefficient*

$$\gamma^{(z)} := \mathbb{1}_{\{\kappa^{(z)}=0\}} + \kappa^{(z)}, \tag{6}$$

so that Equation (5) rewrites compactly as

$$dz_t \mid \Delta_t = \big(\gamma^{(z)}\, \mu^{(z)}_{t,\Delta_t} - \kappa^{(z)}\, z_t\big)\, dt + \sigma^{(z)}\, dW^{(z)}_t. \tag{7}$$

For real interest rates, the two-factor structure is preserved, with a scenario-conditioned long-run mean:

$$\begin{aligned} dr_t \mid \Delta_t &= \kappa^{(r)}\big(l_t - r_t\big)\, dt + \sigma^{(r)}\, dW^{(r)}_t, \\ dl_t \mid \Delta_t &= \kappa^{(l)}\big(\mu^{(r)}_{t,\Delta_t} - l_t\big)\, dt + \sigma^{(l)}\, dW^{(l)}_t. \end{aligned} \tag{8}$$

For real estate returns, two cases are considered depending on the availability of scenario-specific projections.

Case 1: If the factor is explicitly projected in the climate scenarios, a generalized Hull–

White dynamic analogous to (5) is adopted (with $z_t = m_t$ and $\kappa^{(m)} \geq 0$).
Case 2: Otherwise, the real estate return is linked to inflation via:

$$dm_t \mid \Delta_t = \kappa^{(m)}\big(\mu^{(m)} - m_t\big)\, dt + \alpha^{(m)}\, dq_t + \sigma^{(m)}\, dW_t^{(m)}. \tag{9}$$

Equity returns retain the decomposition (3), with the risk premium following the Hardy model (4) and the log-dividend yield and log- Credit spread following the Ornstein-Uhlenbeck dynamics (1). This choice rests on the assumption that climate scenarios affect equities primarily through the nominal rate channel (inflation and real rates).

The following assumptions are imposed. The risk premium noise process $W_t^{(x)}$, the scenario Markov chain (Δ_t), the equity regime Markov chain (ρ_t), and the Brownian vector $(W_t) = \big(W_t^{(c)}, W_t^{(r)}, W_t^{(l)}, W_t^{(m)}, W_t^{(q)}\big)^\top$ are mutually independent. The quadratic covariation matrix of the Brownian vector satisfies $d\langle W\rangle_t = \Sigma_W\, dt = LL^\top\, dt$, where L is the Cholesky decomposition of Σ_W.

Under Case 1, the model's dependency cascade can be represented by the following diagram:

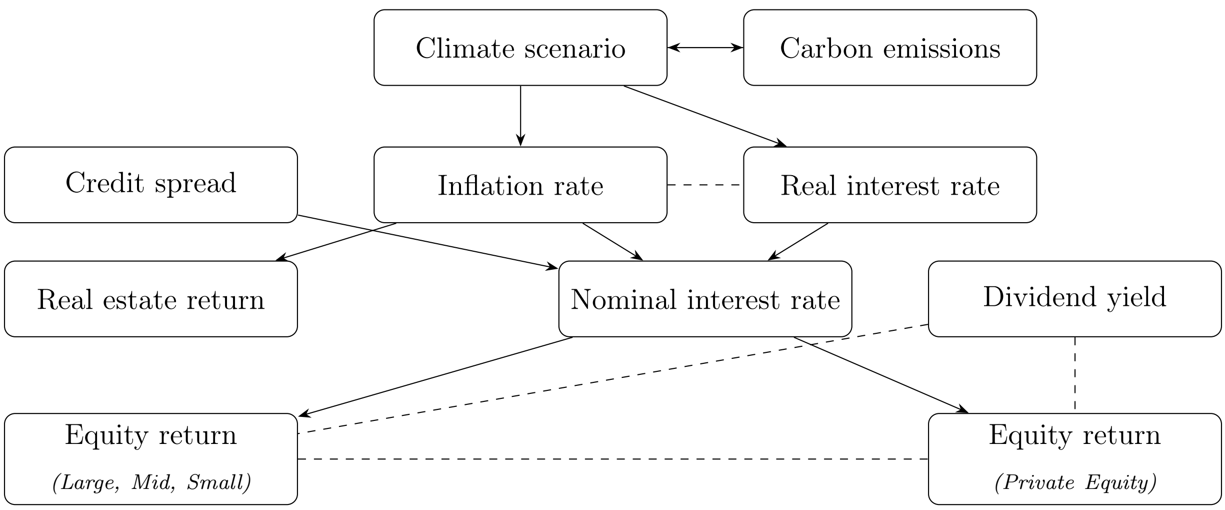

3.3 Latent scenario filtering

Consistent with standard practice, we assume the climate scenario remains fixed once set in motion (Flora and Tankov, 2023). This amounts to setting $P = \mathrm{Id}$, so that the sequence (Δ_t) is time-invariant and simply denoted Δ.

Because the true transition scenario is unobservable, it must be inferred from available data. A primary objective of the modeling framework is therefore to allow the economic agent to filter the noisy signals embedded in these observations and dynamically infer the probability of being in a given scenario j.

Given the model parameters, the objective is to compute the conditional distribution of Δ given the available information. At discrete times $t_0 < t_1 < \cdots$, denote

$o_{t_n} = (c_{t_n}, r_{t_n}, l_{t_n}, m_{t_n}, q_{t_n})$ and $\mathcal{F}_n = \sigma\{o_{t_0}, \ldots, o_{t_n}\}$; the equity process s_t is a measurable function of (q_t, r_t, x_t) with x_t independent of Δ, so it carries no marginal information about the scenario and can be dropped from the filter. Let $\pi_n = (\mathbb{P}(\Delta = j \mid \mathcal{F}_n))^{\top}_{j=1,\ldots,k}$. Bayes' rule gives

$$\pi_n = \frac{\pi_{n-1} \odot \boldsymbol{f}_n}{\mathbf{1}^{\top}(\pi_{n-1} \odot \boldsymbol{f}_n)}, \qquad \boldsymbol{f}_n = \big(f(o_{t_n} \mid \Delta = j, \mathcal{F}_{n-1})\big)^{\top}_{j=1,\ldots,k}, \tag{10}$$

where $\odot$ denotes the Hadamard product and $f(o_{t_n} \mid \Delta = j, \mathcal{F}_{n-1})$ is the scenario-conditional multivariate Gaussian density derived in Appendix B.

The exact computation of $\boldsymbol{f}_n$ from the full multivariate density is numerically expensive. We propose to approximate the conditional distribution by filtering solely on the σ-algebra $\sigma(c_{t_0}, \ldots, c_{t_n})$, using only the decarbonization signal.

This approximation is justified on two grounds. First, as the primary variable governed by the NGFS scenarios, the decarbonization process c_t provides the most direct proxy for scenario inference. Second, projections for other risk factors (inflation, interest rates, real estate) are more speculative and highly sensitive to IAM modeling choices. Including them in the filtration process could introduce unnecessary noise and impair the filter's performance.

Under this approximation, The recursion (10) is preserved, with $\boldsymbol{f}_n$ replaced by

$$\boldsymbol{f}_n^{(c)} = \Big(\varphi\big(c_{t_n};\, e^{-\delta_n \kappa^{(c)}} c_{t_{n-1}} + \Psi(\kappa^{(c)}, \delta_n)\gamma^{(c)} \mu^{(c)}_{t_{n-1},j},\ (\sigma^{(c)})^2 \Psi(2\kappa^{(c)}, \delta_n)\big)\Big)^{\top}_{j=1,\ldots,k}, \tag{11}$$

where $\varphi(\cdot\,; \mu, v)$ is the univariate Gaussian density with mean μ and variance v, and $\Psi(\kappa, \delta) = (1 - e^{-\kappa\delta})/\kappa$ with continuous extension $\Psi(0, \delta) = \delta$.

4 Model estimation

The model parameters are *a priori* unknown and must be inferred from historical data. Let $[0, T]$ denote the sample window and T_0 the beginning of the NGFS projections ($T_0 = 2020$ in the empirical work). Over $[0, T_0]$ all scenarios share a common past, so the mean-reversion levels are scenario-independent:

$$\mu^{(z)}_{t,j} = \mu^{(z)}, \qquad \forall\, t \leq T_0,\ \forall\, j \in \{1, \ldots, k\}. \tag{12}$$

For factors with exogenous post-T_0 trends (inflation, long rate, and real estate under Case 1), $\mu^{(z)}$ is the constant mean over $[0, T_0]$ and the scenario-specific levels $\mu^{(z)}_{t,j}$ for $t > T_0$ are imported from the NGFS projections. For factors without an exogenous forward trend (dividends, real estate under Case 2), $\mu^{(z)}$ is the long-run mean over the full sample.

Calibration proceeds in two stages: factor-by-factor maximum-likelihood estimation on $[0, T_0]$, followed by a multivariate Expectation–Maximization refinement on $[0, T]$ that accounts for the latent Δ. We also perform estimations over $[0, T]$ assuming a fixed, known scenario to analyze parameter changes.

Due to a lack of data, our analysis omits credit spreads and dividends. For numerical purposes, credit spreads are assumed to be integrated directly into real rates.

4.1 Fixed-scenario estimation

When the scenario is known, calibration proceeds sequentially. We first estimate each risk-factor process separately via maximum likelihood (ML), then infer cross-process correlations from the residuals. Because $\mu_{t,i}^{(z)}$ is scenario-specific beyond T_0, the resulting estimates remain scenario-dependent when the full sample is used.

The decarbonization signal c_t is extracted from aggregate GHG emissions as

$$c_t \approx \Delta t^{-1} \log(E_c(t)/E_c(t - \Delta t)),$$

where $E_c(t)$ is the instantaneous emission flow. Using annual EU-27 data over 1980–2024, the exact discretization of (7) with $\delta = 1$ year,

$$c_{t_n} = e^{-\delta\kappa^{(c)}} c_{t_{n-1}} + \Psi(\kappa^{(c)}, \delta)\, \gamma^{(c)}\, \mu_{t_{n-1},\Delta}^{(c)} + \sigma^{(c)} \left[\Psi(2\kappa^{(c)}, \delta)\right]^{1/2} \varepsilon_n^{(c)}, \tag{13}$$

is estimated under three nested specifications: unconstrained OU, Brownian motion ($\kappa^{(c)} = 0$), and NGFS-conditioned estimation. Table 1 reports the parameter estimates. The unconstrained OU estimate $\hat{\kappa} = 14$ implies that the autoregressive coefficient $e^{-\delta\hat{\kappa}}$ collapses to zero at annual frequency, so the process degenerates into a Brownian motion with independent increments. The Brownian specification is therefore retained; residual diagnostics confirm normality (Shapiro–Wilk $p > 0.2$) and absence of autocorrelation.

Table 1: Estimated parameters of the decarbonization process under competing specifications.

	OU	BM	Net Zero 2050	Delayed Trans.	NDCs	Current Pol.
$\hat{\kappa}$	14.000	—	—	—	—	—
$\hat{\mu}$	-1.015	-1.015	-1.110	-1.110	-1.110	-1.110
$\hat{\sigma}$	17.069	3.225	3.349	3.244	3.300	3.244
p-Shapiro–Wilk	0.236	0.236	0.427	0.284	0.369	0.284
Log-likelihood	−2.590	−2.590	−2.628	−2.596	−2.613	−2.596
R^2	0.000	0.000	−0.077	−0.011	−0.047	−0.011

Based on the estimated parameters, we projected annual GHG emissions from 2025 to 2050 using 1,000 simulations under the NGFS scenarios. Figure 2 plot these trajectories for the *Current Policies* and *Net Zero 2050* scenarios. Consistent with the trend of the last decade, the *Current Policies* scenario projects a partial reduction in emissions of roughly 40% over 25 years, with significant dispersion. Conversely, the *Net Zero 2050* scenario shows a strict convergence to zero as expected, accompanied by a sharp decline in emission volatility.

Figure 2: Future evolution of European GHG emissions under Current Policy and Net Zero 2050 NGFS scenario.

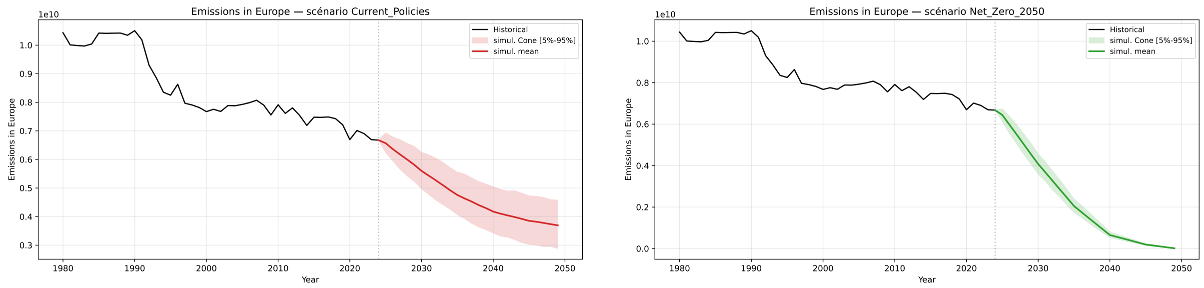

The inflation process is estimated from the annual French consumer price index (CPI) as

$$q_t \approx \Delta t^{-1} \log(\mathrm{CPI}(t)/\mathrm{CPI}(t-\Delta t))$$

and estimated by the same method on French data over 1980–2025. Table 2 compares the unconditional model to the scenario-conditioned specifications. The unconditional model fails to capture the historical volatility of inflation ($R^2 \approx 0.17$, Shapiro–Wilk $p < 0.01$), whereas the scenario-conditioned model raises the explanatory power to $R^2 \approx 0.66$ and pass Gaussian residuals. Explicitly modeling the structural trajectory absorbs the deterministic shocks and leaves only Gaussian noise. This discrepancy stems primarily from the significant inflation surge between 2020 and 2024, driven by the COVID-19 pandemic and the Russo-Ukrainian geopolitical crisis. A constant drift, smoothed over the entire estimation period, cannot absorb these extreme observed shocks. In contrast, the post-2020 scenario pathways inherently integrate these structural breaks into their trajectories.

Table 2: Estimated parameters of the French inflation process.

	No scenario	Net Zero 2050	Delayed Trans.	NDCs	Current Pol.
$\hat{\kappa}$	0.873	1.875	1.827	1.838	1.828
$\hat{\mu}$	1.785	1.430	1.429	1.429	1.429
$\hat{\sigma}$	1.770	1.530	1.520	1.524	1.520
p-Shapiro–Wilk	0.000	0.921	0.914	0.911	0.913
Log-likelihood	-1.615	-1.171	-1.176	-1.176	-1.176
R^2	0.174	0.660	0.656	0.656	0.656

Real estate returns are estimated from the annual French residential house price index.

Three specifications are compared: the inflation-coupled Case 2 model (9) (table 3), a pure OU specification (table 4), and a Brownian motion specification (table 5). The OU specification under Case 1 is preferred: it delivers normal residuals across all scenarios (Shapiro–Wilk $p \geq 0.98$), slightly higher explanatory power than the BM specification, and avoids the over-parameterization of Case 2 whose cross-correlation with inflation is poorly identified on the available sample.

Table 3: Estimated parameters of the French residential real estate process with PC model under French inflation latent factor

Param. & Metric	**No scenario**	**Net Zero 2050**	**Delayed Trans.**	**NDCs**	**Current Pol.**
$\hat{\kappa}$	0.283	0.283	0.283	0.283	0.283
$\hat{\mu}$	3.494	5.495	5.498	5.497	5.498
$\hat{\sigma}$	4.996	4.000	4.008	4.006	4.008
$\hat{\alpha}$	2.213	1.370	1.386	1.382	1.386
$\hat{\rho}$	-0.690	-0.420	-0,423	-0.422	-0,423
p-Shapiro-Wilk	0.805	0.848	0.848	0.848	0.848
Log-likelihood	-3.336	-3.904	-3.885	-3.888	-3.885
R^2	0.595	0.592	0.593	0.593	0.593

Table 4: Estimated parameters of the French residential real estate process under OU model

Param. & Metric	**No scenario**	**Net Zero 2050**	**Delayed Trans.**	**NDCs**	**Current Pol.**
$\hat{\kappa}$	0.335	0.395	0.368	0.372	0.368
$\hat{\mu}$	2.956	4.213	4.203	4.205	4.203
$\hat{\sigma}$	4.259	4.291	4.292	4.292	4.292
p-Shapiro-Wilk	0.887	0.995	0.980	0.983	0.980
Log-likelihood	-2.709	-2.690	-2.702	-2.701	-2.702
R^2	0.512	0.530	0.518	0.520	0.518

Table 5: Estimated parameters of the French residential real estate process under BM model

Param. & Metric	**No scenario**	**Net Zero 2050**	**Delayed Trans.**	**NDCs**	**Current Pol.**
$\hat{\mu}$	3.632	4.320	4.320	4.320	4.320
$\hat{\sigma}$	5.204	4.948	5.041	5.028	5.041
p-Shapiro-Wilk	0.748	0.729	0.807	0.779	0.807
Log-likelihood	-3.068	-3.018	-3.036	-3.034	-3.036
R^2	0.000	0.095	0.061	0.066	0.061

Long-term and short-term real interest rates are estimated using proxies from French 10-year nominal government bonds (OAT) and 3-month fixed-rate treasury bills (BTF), respectively. Data spanning 1980–2025 is netted of French CPI inflation to obtain real rates. The two-factor Vasicek system (8) for real rates is calibrated by maximum likelihood on the exact discretization of the pair (r_t, l_t) derived in Equations 34 and 35. The NGFS-conditioned long-rate calibration mirrors the inflation pattern, with R^2 improving from 0.68 to 0.74. This improvement shares the same underlying cause as inflation: real interest rates dropped significantly when inflation rose at a faster pace than nominal rates, a structural shift that NGFS scenarios capture better than an unconditional model.

Table 6: Estimated parameters of the French long-term interest rate process across baseline and NGFS scenarios.

Param. & Metric	**No scenario**	**Net Zero 2050**	**Delayed Trans.**	**NDCs**	**Current Pol.**
$\hat{\kappa}$	0.222	0.434	0.426	0.427	0.426
$\hat{\sigma}$	1.279	1.262	1.277	1.276	1.277
$\hat{\mu}$	0.683	1.093	1.085	1.086	1.085
p-Shapiro–Wilk	0.490	0.198	0.132	0.133	0.132
Log-likelihood	-1.558	-1.450	-1.465	-1.464	-1.465
R^2	0.681	0.743	0.735	0.736	0.735

Table 7: Estimated parameters of the French short-term interest rate process across baseline and NGFS scenarios.

Param. & Metric	**No scenario**	**Net Zero 2050**	**Delayed Trans.**	**NDCs**	**Current Pol.**
$\hat{\kappa}$	0.174	0.249	0.247	0.247	0.247
$\hat{\sigma}$	1.594	1.579	1.583	1.583	1.583
$\hat{\rho}$	0.651	0.486	0.496	0.495	0.496
p-Shapiro–Wilk	0.016	0.015	0.015	0.015	0.015
Log-likelihood	-2.177	-2.331	-2.320	-2.321	-2.320
R^2	0.259	0.258	0.258	0.258	0.258

We proxy equity risk with the CAC 40 index, using annual data from 1980 to 2025. Given the limited sample size (45 data points), we consider a degenerate form of the Hardy model, reducing it to an arithmetic Brownian motion. Indeed, achieving a consistent estimation of the transition matrix is known to be a difficult problem with a limited sample. The equity risk premium is, by construction, independent of the climate scenario.

Table 8: Estimated parameters of the French equity return (risk premium) process across baseline and NGFS scenarios.

$\hat{\mu}$	$\hat{\sigma}$	p-Shapiro–Wilk	Log-likelihood	R^2
1.786	20.818	0.107	-4.455	0.000

Table 9 presents the estimated correlation matrix under the *Current Policies* scenario.

Table 9: Unconditional correlation matrix

	eu_em	**fr_inf**	**fr_sr**	**fr_lt**	**fr_re**	**fr_eq**
Emission	1.000	-0.158	0.116	0.070	0.324	0.170
Inflation	-0.158	1.000	-0.381	-0.421	-0.070	-0.418
Real Short-rate	0.116	-0.381	1.000	0.496	-0.281	0.186
Real Long-rate	0.070	-0.421	0.496	1.000	-0.145	0.105
Real estate index	0.324	-0.070	-0.281	-0.145	1.000	-0.007
Equity prime index	0.170	-0.418	0.186	0.105	-0.007	1.000

4.2 EM calibration under scenario uncertainty

When Δ is treated as a latent variable, the two-stage procedure applies. Let

$$\theta = \big((\kappa^{(z)})_z,\ (\sigma^{(z)})_z,\ (\mu^{(z)})_z,\ \Sigma_W,\ \pi\big), \qquad z \in \{c, q, r, l, m\},$$

denote the parameter vector. Estimation is performed via the Expectation-Maximization (EM) algorithm, initialized with the pre-scenario estimate $\theta^{(0)}$ (derived as in the fixed-scenario procedure, but restricted to the period $[0, T_0]$) and a uniform prior $\pi_j^{(0)} = 1/k$, which assumes no prior knowledge regarding the initial scenario.

At iteration $l+1$, the E-step computes the expected complete-data log-likelihood

$$Q(\theta \mid \theta^{(l)}) = \sum_{j=1}^{k} \pi_{j|T}^{(l)} \left[\sum_{n=1}^{T} \log f_\theta(o_{t_n} \mid \Delta = j, \mathcal{F}_{n-1}) + \log \pi_j \right], \tag{14}$$

where $\pi_{j|T}^{(l)} = \mathbb{P}_{\theta^{(l)}}(\Delta = j \mid O_T)$ is the smoothed scenario probability delivered by the filter (10), and $f_\theta(\cdot \mid \Delta = j, \mathcal{F}_{n-1})$ is the scenario-conditional Gaussian density given by (33).

The M-step maximizes Q in θ. The initial-distribution update is explicit, $\pi_j^{(l+1)} = \pi_{j|T}^{(l)}$; the remaining parameters are obtained as minimizers of

$$\sum_{j=1}^{k} \pi_{j|T}^{(l)} \sum_{n=1}^{T} \Big[\log\det \Sigma_\varepsilon + \big(o_{t_n} - \Phi_{n-1} o_{t_{n-1}} - g_{n,j}\big)^\top \Sigma_\varepsilon^{-1} \big(o_{t_n} - \Phi_{n-1} o_{t_{n-1}} - g_{n,j}\big) \Big], \tag{15}$$

where Φ_{n-1}, $g_{n,j}$ and Σ_ε embed the VAR representation of the discretized model obtained from (32). The algorithm iterates E and M until the log-likelihood converges; the EM machinery guarantees monotonic increase of the observed likelihood at each iteration.

The estimated parameters are reported in Tables 10 and 11. To reduce computational costs, the covariance matrix was fixed to its estimated values, as shown in Table 9.

Table 10: Estimated parameters for the different models

Variable	μ	κ	σ	ρ
Emission	-1.105	0.0000	3.236	-
Inflation	1.438	1.825	1.523	-
Real Short-rate	-	0.248	1.588	0.496
Real Long-rate	1.079	0.422	1.280	-
Real estate index	4.233	0.370	4.302	-
Equity prime index	1.726	0.0000	19.873	-

Based on the 2020–2025 carbon emission dynamics, the estimated initial probabilities, Tab. 11, lean towards a latent scenario between *Current Policies* and *NDCs*.

Table 11: NGFS scenario initial probabilities (π_i).

	Net Zero 2050	**Delayed Trans.**	**NDCs**	**Current Pol.**
π_i	0.00	0.49	0.02	0.49

To evaluate the performance of the filter, we simulated the risk factors for a given transition scenario and ran our filter (see Figure 3). We first observed that the filter's performance is nearly identical whether we use only the decarbonization rate as a filtering proxy or integrate all risk factors. Second, during the initial filtering period (up to 2030), the filter can struggle to distinguish the latent scenario among initially similar pairs (such as Delayed Transition vs. Current Policies, or Net Zero vs. NDCs). However, from 2035 onward, the latent scenario is consistently identified with a probability close to 1. This early ambiguity aligns with Flora and Tankov (2023), who note that scenarios can be difficult to distinguish at the beginning, an ambiguity that can systematically reduce asset values during the decision-making process.

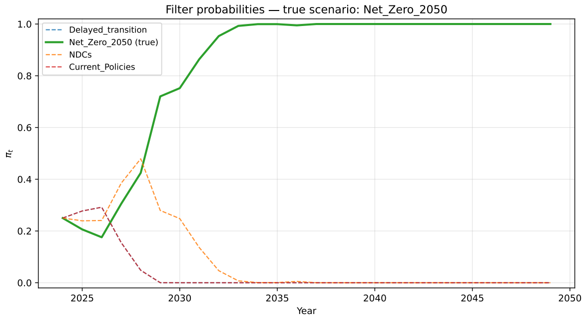

(a) Net Zero 2050

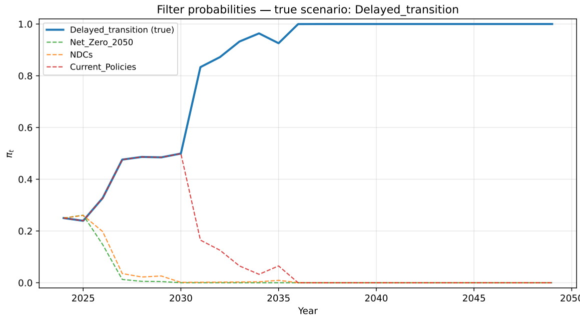

(b) Delayed transition

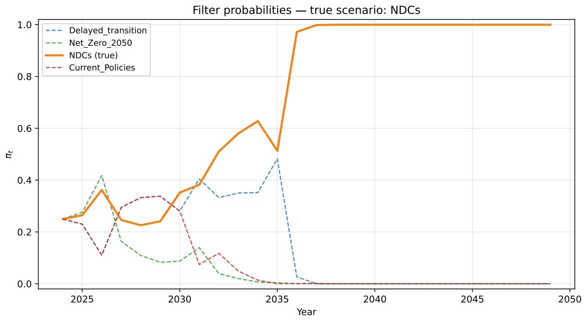

(c) NDCs

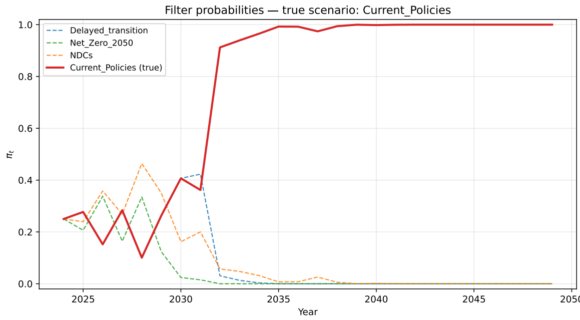

(d) Current Policies

Figure 3: Evolution of the filtered probabilities for each scenario along a single simulation path.

5 Portfolio allocation under climate scenarios

This section presents a dynamic asset-liability management (ALM) framework for a representative non-life insurance portfolio. We aim to quantify the financial impact of transition risk on the balance sheet and identify management strategies that optimize risk metrics, liquidity, and overall financial performance. The stylized balance sheet matches stochastic underwriting cash flows and an own funds buffer against a three-asset portfolio comprising equities, real estate, and a duration-targeted bond book.

5.1 Asset–liability framework

The non-life insurer is initialized at $t = 0$ with a total asset value of M. At any time step $t \in \{0, 1, \dots, H\}$, the balance sheet comprises invested assets W_t, best-estimate technical provisions L_t, and own funds $K_t = W_t - L_t$. Assuming an initial equity ratio of $\alpha_K \in (0, 1)$, the initial conditions are:

$$W_0 = M, \qquad L_0 = (1 - \alpha_K)M, \qquad K_0 = \alpha_K M$$

The strategic asset allocation is governed by a target bond weight $\alpha_B \in (0, 1)$ and an equity share within the non-bond portfolio, denoted by $\beta \in (0, 1)$. Letting $\gamma :=$

$(1-\beta)(1-\alpha_B)$ represent the residual real estate allocation, the mark-to-market target values for the three asset classes are given by:

$$V_t^{\text{bonds}} = \alpha_B W_t, \qquad V_t^{(s)} = \beta(1-\alpha_B)W_t, \qquad V_t^{(m)} = \gamma W_t \tag{16}$$

The insurer seeks to restore this allocation at each rebalancing date, subject to prevailing liquidity and accounting constraints.

The bond portfolio consists of fixed-rate nominal bonds subject to a hold-to-maturity (HTM) accounting convention. Voluntary sales are not allowed; the portfolio only reduces through maturities or forced liquidations to cover cash deficits. To maintain a stable interest-rate exposure and a duration gap consistent with liability flows, a duration-targeting rule is applied. At each rebalancing date, new bonds are selected to restore the overall Macaulay duration to a constant target $\mathcal{T}$.

Equities are modeled as liquid and frictionless. Real estate investments incur a proportional haircut $h \in [0,1)$ upon sale, reflecting the illiquidity and transaction costs of secondary property markets.

On the liability side, assuming a stationary insured risk (Assumption 1), provisions remain constant in real terms.

Assumption 1. *The insured population and the probabilistic structure of claim arrivals and severities are stationary over $[0,H]$. In particular, the expected policyholder stock, the expected claim frequency per policy, and the real severity distribution of ultimate losses are constant in real terms.*

Consequently, the nominal liability L_t grows with the inflation rate $\tilde{q}_t$:

$$L_t = L_{t-1}(1+\tilde{q}_t) = L_0 I_t, \qquad t = 1,\ldots,H., \qquad I_t = \prod_{s=1}^{t}(1+\tilde{q}_s). \tag{17}$$

This implies that climate scenarios influence the liability balance solely via the inflation channel.

The annual underwriting margin, derived from the combined ratio, is modeled as a stochastic fraction of the technical provisions:

$$\xi_t = \big(a_0 + b_0\varepsilon_t\big)L_{t-1}, \qquad \varepsilon_t \overset{\text{i.i.d.}}{\sim} \mathcal{N}(0,1), \tag{18}$$

where $a_0 \in \mathbb{R}$ and $b_0 > 0$ denote the expected margin and its standard deviation, respectively. Furthermore, underwriting shocks ε_t are assumed to be independent to market factors.

At each time step t, the net cash flow is given by $\Phi_t = \mathcal{C}_t + \xi_t$, where $\mathcal{C}_t$ denotes the bond coupons. If $\Phi_t < 0$, a liquidation waterfall is triggered: equities are sold first, followed by real estate subject to the haircut, and finally bonds, until the deficit is covered or insolvency occurs. Conversely, if $\Phi_t \geq 0$, the surplus cash is reinvested to realign with the strategic targets (16). Due to the HTM restrictions on bonds, equity sales are used as the primary adjustment mechanism.

Defining the investment return as $R_t^{\text{inv}} = (W_t - W_{t-1} - \xi_t)/W_{t-1}$, the law of motion for own funds is:

$$K_t - K_{t-1} = R_t^{\text{inv}} W_{t-1} + \xi_t - \tilde{q}_t L_{t-1}. \tag{19}$$

5.2 Performance and solvency metrics

For each scenario j, n trajectories are simulated. The bankruptcy time is defined as:

$$\tau_j(\omega) = \inf\{t \geq 1 : K_t(\omega) \leq 0\}, \tag{20}$$

where $\tau_j(\omega) = +\infty$ if the insurer remains solvent throughout the horizon H. To evaluate financial performance independently of default events, investment metrics are calculated only over the subset of solvent paths Ω_j^{solv}, while prudential metrics are computed across the full sample.

The mean per-period investment return is given by:

$$\bar{R}_j = \frac{1}{H} \sum_{t=1}^{H} \bar{R}_{j,t}, \qquad \text{where} \qquad \bar{R}_{j,t} = \frac{1}{n_j^{\text{solv}}} \sum_{\omega \in \Omega_j^{\text{solv}}} R_t^{\text{inv}}(\omega), \tag{21}$$

and investment risk is quantified via the following conditional volatility:

$$\hat{\sigma}_j^{\text{cond}} = \frac{1}{H} \sum_{t=1}^{H} \hat{\sigma}_{j,t}^{\text{cond}}, \qquad \text{where} \quad \left(\hat{\sigma}_{j,t}^{\text{cond}}\right)^2 = \frac{1}{n_j^{solv}} \sum_{\omega \in \Omega_j^{\text{solv}}} \left(R_t^{\text{inv}}(\omega) - \bar{R}_{j,t}\right)^2. \tag{22}$$

Transition scenarios incorporate deterministic trends that a pooled variance would conflate with financial risk. By averaging cross-sectional dispersions over time, we remove these predictable components to isolate the stochastic variation inherent to the risk factors.

Prudential outcomes are evaluated using the terminal funding ratio and the empirical bankruptcy probability:

$$\text{FR}_H(\omega) = \frac{W_H(\omega)}{L_H(\omega)} = 1 + \frac{K_H(\omega)}{L_H(\omega)}, \tag{23}$$

$$\hat{p}_j^{\text{bankr}} = \frac{1}{n} \sum_{\omega=1}^{n} \mathbf{1}\{\tau_j(\omega) \leq H\}. \tag{24}$$

5.3 Numerical results

For our numerical applications, we calibrate the parameters to $(\alpha_B, \beta, a_0, b_0, h) = (0.85, 0.40, 0.01, 0.03, 0.05)$ to closely mirror operational practices. Reflecting risk aversion, liquidity requirements, and regulatory constraints, non-life insurance portfolios are predominantly composed of bonds, 70% to 90% of total assets, with the remaining allocation distributed evenly between equities and real estate. The initial liability M is set to 1 billion euros, assuming a 15% equity capital ratio.

While French inflation and real estate indices follow relatively similar paths across scenarios, long-term interest rate dynamics exhibit significant heterogeneity (see Figure 1). Rates are substantially higher in the Net Zero 2050 scenario, with a marked divergence emerging after 2035. Given the bond-heavy nature of the portfolio, our analysis focuses on the impact of bond duration on financial performance and solvency metrics.

As expected, the results highlight a strong dependence of financial solvency and profitability on yield curve dynamics and portfolio duration. Table 12 reports the simulated metrics across the four NGFS scenarios for a 1-year target duration. It shows that the Net Zero scenario portfolio outperforms others by over 25 bp in annual mean return. This superior performance is accompanied by reduced conditional volatility and improved prudential metrics, such as a lower probability of default and a higher funding ratio. We attribute this outperformance to the portfolio's capacity to capture the sustained high yields characterizing the Net Zero pathway from 2030 onward. From a macroeconomic perspective, this upward shift reflects the risk premium associated with the massive investments required for an orderly transition.

Conversely, increasing the target duration reduces this advantage. By locking a larger share of funds into long-term bonds as early as 2025, the insurer loses the flexibility to capitalize on subsequent rate hikes. Consequently, portfolio returns become anchored to the initial yield curve, compressing performance spreads across scenarios (see Figure 4). This duration-driven lock-in effect can be detrimental to solvency: as liabilities continue to absorb inflation shocks without corresponding yield compensation on the asset side, the funding ratio systematically deteriorates (see Figure 5).

Table 12: Cross-scenario portfolio performance and solvency metrics. Values are taken at $T = 2025$ and $\mathcal{T} = 1$.

Metric	**Net Zero 2050**	**Delayed Trans.**	**NDCs**	**Current Pol.**
Mean return $\bar{R}_j$	4.97%	4.71%	4.72%	4.63%
	(1.07%)	(1.05%)	(1.04%)	(1.05%)
Cond. volatility $\hat{\sigma}_j^{\text{cond}}$	3.49%	3.54%	3.53%	3.57%
	(0.58%)	(0.56%)	(0.57%)	(0.56%)
Terminal funding ratio FR_H	1.999	1.833	1.864	1.839
	(0.596)	(0.546)	(0.541)	(0.550)
Bankruptcy prob. $\hat{p}_j^{\text{bankr}}$	2.30%	3.80%	3.60%	5.20%
	(15.00%)	(19.13%)	(18.64%)	(22.21%)
Underfunding prob. $\hat{p}_j^{\text{under}}$	14.90%	19.00%	18.30%	20.30%
	(35.63%)	(39.25%)	(38.69%)	(40.24%)
Mean ΔK_{1y} at $T = H$	86 163 499	66 168 319	62 132 489	59 146 546
	(86 780 709)	(91 864 959)	(84 307 154)	(77 616 608)

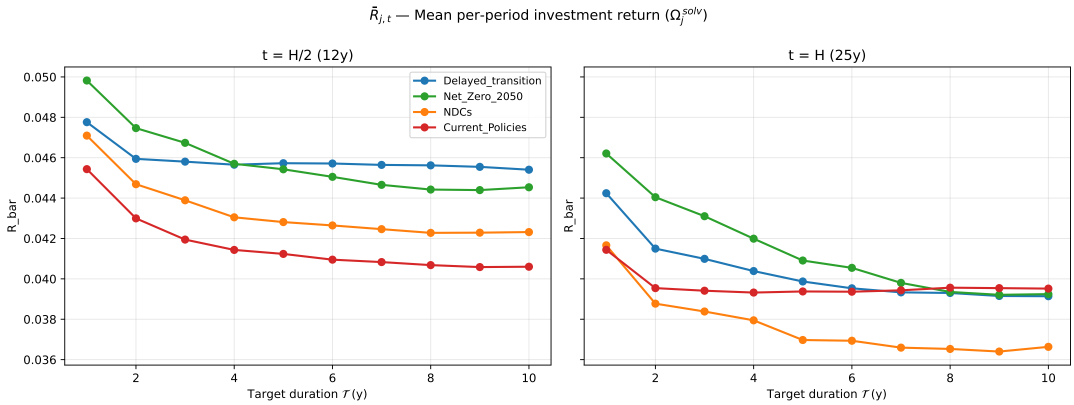

Figure 4: Financial return rate by target maturity at horizons T = 2037 and T = 2050 across scenarios.

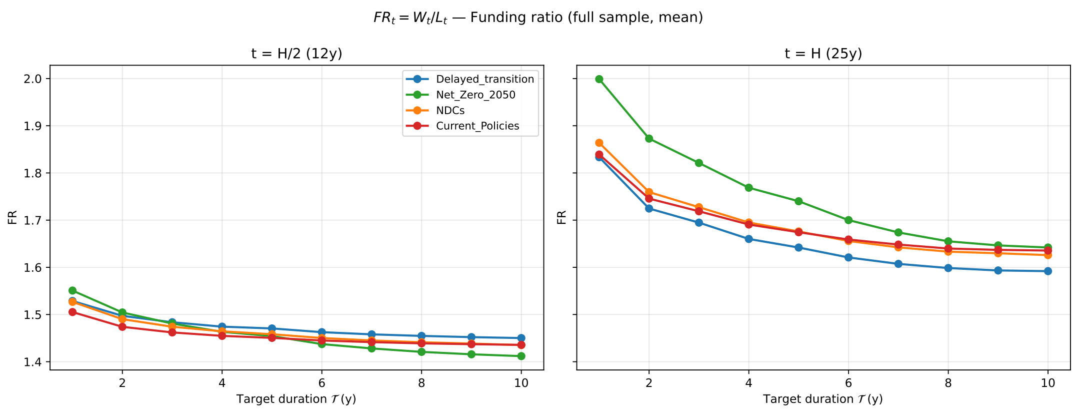

Figure 5: Funding ratio by target maturity at horizons T = 2037 and T = 2050 across scenarios.

5.4 Limitations and perspectives

Two primary caveats should be considered when interpreting these findings. First, the framework does not explicitly incorporate physical climate damages, such as the increased frequency of natural disasters expected under "hot-house" scenarios (Current Policies and NDCs). As technical provision dynamics are assumed to be stationary in this study, incorporating exacerbated physical risks would likely widen the performance gap of the Net Zero scenario and increase default probabilities for high-warming trajectories. Therefore, these results should be viewed as a conservative lower bound of the financial benefits of an orderly transition.

Second, the asset modeling remains highly aggregated, representing the portfolio through generic indices. In practice, insurance portfolios are far more complex. Integrating sector-specific dynamics, distinguishing between green assets and "brown" stranded assets, would allow for a more nuanced assessment of transition impacts and a more exhaustive evaluation of investment risks.

Building on these results, future research will extend this framework to life insurance portfolios. Life insurance introduces deeper asset-liability interdependencies due to embedded options and market-sensitive policyholder behavior. Moreover, the long-term nature of liabilities necessitates more granular asset modeling to capture the specific risks of long-duration management.

References

Ahlgrim, K.C., D'Arcy, S.P., and Gorvett, R.W. (2005). Modeling Financial Scenarios: A Framework for the Actuarial Profession. *Proceedings of the Casualty Actuarial Society*, 92, 177–238.

Wilkie, A.D. (1986). A Stochastic Investment Model for Actuarial Use. *Transactions of the Faculty of Actuaries*, 39, 341–403.

Hamilton, J.D. (1989). A New Approach to the Economic Analysis of Nonstationary Time Series and the Business Cycle. *Econometrica*, 57(2), 357–384.

Hardy, M.R. (2001). A Regime-Switching Model of Long-Term Stock Returns. *North American Actuarial Journal*, 5(2), 41–53.

NGFS (2019). *A Call for Action: Climate Change as a Source of Financial Risk*. Paris: NGFS Secretariat.

NGFS (2020). *NGFS Climate Scenarios for Central Banks and Supervisors — Phase I*. Paris: NGFS.

NGFS (2023). *NGFS Climate Scenarios for Central Banks and Supervisors — Phase IV.* Paris: NGFS.

NGFS (2024a). *NGFS Climate Scenarios for Central Banks and Supervisors — Phase V.* Paris: NGFS.

ACPR (2021). *A First Assessment of Financial Risks Stemming from Climate Change: The Main Results of the 2020 Climate Pilot Exercise.* Analyses et Synthèses No. 122. Paris: Banque de France.

ACPR (2024). *Main Results of the Climate Exercise for the Insurance Sector.* Paris: Banque de France.

Allen, T., Dées, S., Caicedo Graciano, C.M., et al. (2020). Climate-Related Scenarios for Financial Stability Assessment: An Application to France. *Banque de France Working Paper* No. 774.

European Central Bank (2022). *2022 Climate Risk Stress Test.* Frankfurt: ECB Banking Supervision.

Battiston, S., Mandel, A., Monasterolo, I., Schütze, F., and Visentin, G. (2017). A Climate Stress-Test of the Financial System. *Nature Climate Change*, 7(4), 283–288.

Vermeulen, R., Schets, E., Lohuis, M., et al. (2021). The Heat is On: A Framework for Measuring Financial Stress under Disruptive Energy Transition Scenarios. *Ecological Economics*, 190, Article 107205.

Chekriy, K., Kiesel, R., and Stahl, G. (2025). Probabilistic Assessment of Corporate Net-Zero Transition. SSRN Working Paper 5255705.

Flora, M. and Tankov, P. (2023). Green Investment and Asset Stranding under Transition Scenario Uncertainty. *Energy Economics*, 124, Article 106773.

Mazzon, A. and Tankov, P. (2024). Optimal Stopping and Divestment Timing under Scenario Ambiguity and Learning. arXiv:2408.09349.

Trust, S., Joshi, S., Lenton, T., and Oliver, J. (2023). The Emperor's New Climate Scenarios — A Warning for Financial Services. Institute and Faculty of Actuaries / University of Exeter.

Boudreault, M., Clacher, I., Zhou, Q., and Li, J. (2023). A Changing Climate for Actuarial Science (editorial). *Annals of Actuarial Science*, 17(3).

Dione, O. (2025). Design a Climate-Aware Economic Scenario Generator (CA-ESG): Towards a New Macro-Financial Projection Framework. Working Paper, EconomiX (UMR CNRS 7235), Université Paris Nanterre.

Baumstark, L., Bauer, N., Benke, F., et al. (2021). REMIND2.1: Transformation and Innovation Dynamics of the Energy-Economic System. *Geoscientific Model Development*, 14, 6571–6603.

Huppmann, D., Gidden, M., Fricko, O., et al. (2019). The MESSAGEix Integrated Assessment Model and the ix Modeling Platform. *Environmental Modelling & Software*, 112, 143–156.

Calvin, K., Patel, P., Clarke, L., et al. (2019). GCAM v5.1: Representing the Linkages between Energy, Water, Land, Climate, and Economic Systems. *Geoscientific Model Development*, 12, 677–698.

A Closed-form solution for non-autonomous linear SDEs

The multivariate discretization of Appendix B relies on the following standard result, stated and proved for completeness.

Theorem 1. *Let $X_t \in \mathbb{R}^n$ be the solution of*

$$dX_t = \big(A(t) + B(t)\,X_t\big)\,dt + \Sigma\,dW_t, \qquad X_0 = \eta,$$

where $A : \mathbb{R}_+ \to \mathbb{R}^n$ is measurable and integrable on $[0,t]$ for every t, $B : \mathbb{R}_+ \to \mathbb{R}^{n\times n}$ is continuous, $\Sigma \in \mathbb{R}^{n\times m}$, W_t is an m-dimensional Brownian motion, and η is $\mathcal{F}_0$-measurable. Then

$$X_t = \Phi(t,0)\,\eta + \int_0^t \Phi(t,s)\,A(s)\,ds + \int_0^t \Phi(t,s)\,\Sigma\,dW_s,$$

where $\Phi(t,s)$ is the unique matrix-valued solution of $\partial_t\Phi(t,s) = B(t)\,\Phi(t,s)$ with $\Phi(s,s) = I_n$. Without a commutativity assumption on $B(\cdot)$, $\Phi(t,s)$ is the time-ordered exponential $\mathcal{T}\exp\big(\int_s^t B(u)\,du\big)$. If B is constant and diagonalizable, $B = P\,D\,P^{-1}$ with $D = \mathrm{diag}(\lambda_1,\dots,\lambda_n)$, then $\Phi(t,s) = e^{(t-s)B}$ and

$$X_t = e^{tB}\,\eta + \int_0^t e^{(t-s)B}\big(A(s)\,ds + \Sigma\,dW_s\big). \tag{25}$$

In this case, $X_t \mid \eta$ is Gaussian with covariance converging to $\Sigma_\infty = \int_0^\infty e^{sB}\,\Sigma\Sigma^\top e^{sB^\top}\,ds$ if and only if $\mathrm{Re}(\lambda_i) < 0$ for every i.

Proof. Set $Y_t = \Phi(0,t)\,X_t$. By Itô's formula and the defining ODE of Φ,

$$dY_t = \Phi(0,t)\,A(t)\,dt + \Phi(0,t)\,\Sigma\,dW_t.$$

Integrating over $[0,t]$ and multiplying by $\Phi(t,0)$ yields the result via the semigroup property. $\square$

B Multivariate autoregressive representation

We derive the exact discretization of the multivariate risk-factor system of Section 3. Consider the state vector

$$X_t = \begin{bmatrix} c_t & r_t & l_t & m_t & q_t \end{bmatrix}^\top .$$

Conditional on Δ, the dynamics take the generic form $dX_t \mid \Delta = (A_t + BX_t)\,dt + \Sigma\, d\widetilde{W}_t$, with $\widetilde{W}_t$ a standard Brownian motion in $\mathbb{R}^5$ and the matrices A_t, B, Σ depending on the real-estate specification.

B.1 System matrices

Under Case 1 (Hull–White dynamics for real estate), with $\gamma^{(z)}$ as in (6),

$$A_t = \begin{pmatrix} \gamma^{(c)}\,\mu^{(c)}_{t,\Delta} \\ 0 \\ \kappa^{(l)}\,\mu^{(r)}_{t,\Delta} \\ \gamma^{(m)}\,\mu^{(m)}_{t,\Delta} \\ \gamma^{(q)}\,\mu^{(q)}_{t,\Delta} \end{pmatrix}, \quad B = \begin{pmatrix} -\kappa^{(c)} & 0 & 0 & 0 & 0 \\ 0 & -\kappa^{(r)} & \kappa^{(r)} & 0 & 0 \\ 0 & 0 & -\kappa^{(l)} & 0 & 0 \\ 0 & 0 & 0 & -\kappa^{(m)} & 0 \\ 0 & 0 & 0 & 0 & -\kappa^{(q)} \end{pmatrix}, \tag{26}$$

and $\Sigma = D_\sigma\, L$ with $D_\sigma = \mathrm{diag}(\sigma^{(c)}, \sigma^{(r)}, \sigma^{(l)}, \sigma^{(m)}, \sigma^{(q)})$ and L the Cholesky factor of Σ_W. The matrix B is unchanged relative to the original Ahlgrim specification; the modeling assumption acts solely through A_t.

Under Case 2 (inflation-linked real estate),

$$A_t = \begin{pmatrix} \gamma^{(c)}\,\mu^{(c)}_{t,\Delta} \\ 0 \\ \kappa^{(l)}\,\mu^{(r)}_{t,\Delta} \\ \kappa^{(m)}\mu^{(m)} + \alpha^{(m)}\gamma^{(q)}\mu^{(q)}_{t,\Delta} \\ \gamma^{(q)}\,\mu^{(q)}_{t,\Delta} \end{pmatrix}, \quad B = \begin{pmatrix} -\kappa^{(c)} & 0 & 0 & 0 & 0 \\ 0 & -\kappa^{(r)} & \kappa^{(r)} & 0 & 0 \\ 0 & 0 & -\kappa^{(l)} & 0 & 0 \\ 0 & 0 & 0 & -\kappa^{(m)} & -\alpha^{(m)}\kappa^{(q)} \\ 0 & 0 & 0 & 0 & -\kappa^{(q)} \end{pmatrix}, \tag{27}$$

$$\Sigma = \begin{pmatrix} \sigma^{(c)} & 0 & 0 & 0 & 0 \\ 0 & \sigma^{(r)} & 0 & 0 & 0 \\ 0 & 0 & \sigma^{(l)} & 0 & 0 \\ 0 & 0 & 0 & \sigma^{(m)} & \alpha^{(m)}\sigma^{(q)} \\ 0 & 0 & 0 & 0 & \sigma^{(q)} \end{pmatrix} L = D_\sigma\, L. \tag{28}$$

B.2 Diagonalization of the drift matrix

In both cases the eigenvalues of B are $-\kappa^{(c)}, -\kappa^{(r)}, -\kappa^{(l)}, -\kappa^{(m)}, -\kappa^{(q)}$. We assume throughout

$$\kappa^{(r)} \neq \kappa^{(l)}, \qquad \kappa^{(m)} \neq \kappa^{(q)}, \qquad \kappa^{(z)} \geq 0 \text{ for } z \in \{c, m, q\}, \qquad \kappa^{(z)} > 0 \text{ for } z \in \{r, l\},$$

under which $B = P\,D\,P^{-1}$ with $D = \operatorname{diag}(-\kappa^{(c)}, -\kappa^{(r)}, -\kappa^{(l)}, -\kappa^{(m)}, -\kappa^{(q)})$ and

$$P_{\text{Case 1}} = \begin{pmatrix} 1 & 0 & 0 & 0 & 0 \\ 0 & 1 & \dfrac{\kappa^{(r)}}{\kappa^{(r)} - \kappa^{(l)}} & 0 & 0 \\ 0 & 0 & 1 & 0 & 0 \\ 0 & 0 & 0 & 1 & 0 \\ 0 & 0 & 0 & 0 & 1 \end{pmatrix}, \quad P_{\text{Case 2}} = \begin{pmatrix} 1 & 0 & 0 & 0 & 0 \\ 0 & 1 & \dfrac{\kappa^{(r)}}{\kappa^{(r)} - \kappa^{(l)}} & 0 & 0 \\ 0 & 0 & 1 & 0 & 0 \\ 0 & 0 & 0 & 1 & \dfrac{\alpha^{(m)}\kappa^{(q)}}{\kappa^{(q)} - \kappa^{(m)}} \\ 0 & 0 & 0 & 0 & 1 \end{pmatrix}. \tag{29}$$

B.3 Exact discretization

Let $\delta_n = t_n - t_{n-1}$. Assuming A_t is piecewise constant on the time grid, Theorem 1 yields

$$X_{t_n} = e^{\delta_n B}\, X_{t_{n-1}} + \left(\int_0^{\delta_n} e^{sB}\, ds \right) A_{t_{n-1}} + \int_{t_{n-1}}^{t_n} e^{(t_n - s)B}\, \Sigma\, dW_s. \tag{30}$$

Using $B = P\,D\,P^{-1}$,

$$\int_0^{\delta_n} e^{sB}\, ds = P \operatorname{diag}\big(\Psi(\kappa^{(z)}, \delta_n)\big)_z\, P^{-1}, \qquad z \in \{c, r, l, m, q\},$$

where

$$\Psi(\kappa, \delta) := \begin{cases} \dfrac{1 - e^{-\kappa\delta}}{\kappa} & \text{if } \kappa > 0, \\ \delta & \text{if } \kappa = 0, \end{cases} \tag{31}$$

is the continuous extension at $\kappa = 0$. The stochastic integral is a zero-mean Gaussian vector with covariance

$$\Sigma_\varepsilon = P\,(K \odot M)\,P^\top,$$

where $M = P^{-1}\Sigma\Sigma^\top P^{-\top}$, $\Sigma\Sigma^\top = D_\sigma \Sigma_W D_\sigma^\top$, and $K = [\Psi(\kappa^{(i)} + \kappa^{(j)}, \delta_n)]_{i,j}$. The discretized system takes the VAR form

$$X_{t_n} = \Phi_{n-1}\, X_{t_{n-1}} + g_{n,\Delta} + \varepsilon_n, \tag{32}$$

with $\Phi_{n-1} = e^{\delta_n B}$, $g_{n,\Delta} = P\,\mathrm{diag}(\Psi(\kappa^{(z)}, \delta_n))_z\, P^{-1} A_{t_{n-1}}$, and $\varepsilon_n \sim \mathcal{N}(0, \Sigma_\varepsilon)$. The conditional density of X_{t_n} given Δ and $\mathcal{F}_{n-1}$ is therefore

$$f(X \mid \Delta, \mathcal{F}_{n-1}) = \frac{1}{\sqrt{(2\pi)^5 \det \Sigma_\varepsilon}} \exp\left(-\frac{1}{2} (X - \Phi_{n-1} X_{t_{n-1}} - g_{n,\Delta})^\top \Sigma_\varepsilon^{-1} (X - \Phi_{n-1} X_{t_{n-1}} - g_{n,\Delta}) \right). \tag{33}$$

B.4 Univariate projections (Case 1)

For $z \in \{c, l, q, m\}$, the univariate recursion is

$$z_{t_n} = e^{-\delta_n \kappa^{(z)}}\, z_{t_{n-1}} + \Psi(\kappa^{(z)}, \delta_n)\, \gamma^{(z)}\, \mu^{(z)}_{t_{n-1},\Delta} + \widetilde{\sigma}^{(z)}_n\, \varepsilon^{(z)}_n, \tag{34}$$

with $\big(\widetilde{\sigma}^{(z)}_n\big)^2 = (\sigma^{(z)})^2 \Psi(2\kappa^{(z)}, \delta_n)$ and $\varepsilon^{(z)}_n \sim \mathcal{N}(0,1)$. For the short rate, with $a = \kappa^{(r)}/(\kappa^{(r)} - \kappa^{(l)})$,

$$\begin{aligned} r_{t_n} = e^{-\delta_n \kappa^{(r)}}\, r_{t_{n-1}} &+ a\big(e^{-\delta_n \kappa^{(l)}} - e^{-\delta_n \kappa^{(r)}}\big)\, l_{t_{n-1}} \\ &+ \frac{\kappa^{(r)}\kappa^{(l)}}{\kappa^{(r)} - \kappa^{(l)}} \big[\Psi(\kappa^{(l)}, \delta_n) - \Psi(\kappa^{(r)}, \delta_n)\big]\, \mu^{(r)}_{t_{n-1},\Delta} + \widetilde{\sigma}^{(r)}_n\, \varepsilon^{(r)}_n, \end{aligned} \tag{35}$$

with conditional variance

$$\big(\widetilde{\sigma}^{(r)}_n\big)^2 = (\sigma^{(r)})^2 K_{rr} + 2a\, \sigma^{(r)}\sigma^{(l)} \rho_{rl} (K_{rl} - K_{rr}) + a^2 (\sigma^{(l)})^2 (K_{ll} - 2K_{rl} + K_{rr}).$$

Off-diagonal entries of Σ_ε are

$$\begin{aligned} &\text{For } i, j \neq r: \quad (\Sigma_\varepsilon)_{ij} = K_{ij}\, \rho_{ij}\, \sigma^{(i)}\sigma^{(j)}, \\ &\text{For } j \neq r: \quad (\Sigma_\varepsilon)_{rj} = K_{rj}\, \rho_{rj}\, \sigma^{(r)}\sigma^{(j)} + a(K_{lj} - K_{rj})\, \rho_{lj}\, \sigma^{(l)}\sigma^{(j)}. \end{aligned} \tag{36}$$

B.5 Univariate projections (Case 2)

For $z \in \{c, l, q, r\}$, the univariate recursions are unchanged. With $b = \alpha^{(m)}\kappa^{(q)}/(\kappa^{(q)} - \kappa^{(m)})$, the real-estate recursion is

$$\begin{aligned} m_{t_n} = e^{-\delta_n \kappa^{(m)}}\, m_{t_{n-1}} &+ b\big(e^{-\delta_n \kappa^{(q)}} - e^{-\delta_n \kappa^{(m)}}\big)\, q_{t_{n-1}} \\ &+ \Psi(\kappa^{(m)}, \delta_n)\big[\kappa^{(m)}\mu^{(m)} + \alpha^{(m)}\kappa^{(q)}\mu^{(q)}_{t_{n-1},\Delta}\big] \\ &+ b\big[\Psi(\kappa^{(q)}, \delta_n) - \Psi(\kappa^{(m)}, \delta_n)\big]\, \kappa^{(q)}\mu^{(q)}_{t_{n-1},\Delta} + \widetilde{\sigma}^{(m)}_n\, \varepsilon^{(m)}_n, \end{aligned} \tag{37}$$

with conditional variance

$$\big(\widetilde{\sigma}^{(m)}_n\big)^2 = K_{mm}\big[(\sigma^{(m)})^2 + 2\sigma^{(m)}\sigma^{(q)}(\alpha^{(m)} - b)\rho_{mq} + (\alpha^{(m)} - b)^2(\sigma^{(q)})^2\big] + 2bK_{mq}\big[\sigma^{(m)}\sigma^{(q)}\rho_{mq} + (\alpha^{(m)} - b)(\sigma^{(q)})^2$$

C Maximum likelihood estimation of the Hardy equity model

From (3), the observed risk-premium increments satisfy

$$z_i \mid \rho_{t_i} \sim \mathcal{N}\big(\delta\, \mu^{(x)}_{\rho_{t_i}}, \delta(\sigma^{(x)}_{\rho_{t_i}})^2\big),$$

where $\rho_{t_i} \in \{1, \dots, d\}$ is the equity regime at t_i. Let $P = (p_{ij})$ be the transition matrix and $\boldsymbol{\pi}$ its initial distribution; set $\boldsymbol{\theta} = ((\mu^{(x)}_i)_i, (\sigma^{(x)}_i)_i, P)$. The observed-data likelihood factorizes as

$$L_n(\boldsymbol{\theta}) = f_{\boldsymbol{\theta}}(z_1) \prod_{t=2}^{n} f_{\boldsymbol{\theta}}(z_t \mid z_1, \dots, z_{t-1}),$$

with conditional density $f_{\boldsymbol{\theta}}(z_t \mid z_1, \dots, z_{t-1}) = \sum_i \pi_{t|t-1}(i)\, \varphi(z_t; \delta\mu^{(x)}_i, \delta(\sigma^{(x)}_i)^2)$, where $\varphi(\,\cdot\,; m, v)$ is the Gaussian density with mean m and variance v. The filter recursion

$$\boldsymbol{\pi}_{t|t} = \frac{\boldsymbol{\pi}_{t|t-1} \odot \boldsymbol{\varphi}_t}{\mathbf{1}^\top(\boldsymbol{\pi}_{t|t-1} \odot \boldsymbol{\varphi}_t)}, \qquad \boldsymbol{\pi}_{t+1|t} = P^\top \boldsymbol{\pi}_{t|t}, \tag{38}$$

is initialized from the stationary distribution.

Direct maximization is numerically challenging; we apply EM with $(\rho_1, \dots, \rho_n)$ as missing data. The M-step yields

$$\hat{\mu}^{(x)}_i = \frac{\sum_t z_t\, \boldsymbol{\pi}_{t|n}(i)}{\delta \sum_t \boldsymbol{\pi}_{t|n}(i)}, \qquad (\hat{\sigma}^{(x)}_i)^2 = \frac{\sum_t (z_t - \delta\hat{\mu}^{(x)}_i)^2 \boldsymbol{\pi}_{t|n}(i)}{\delta \sum_t \boldsymbol{\pi}_{t|n}(i)}, \tag{39}$$

$$\hat{p}_{ij} = \frac{\sum_t \boldsymbol{\pi}_{t-1,t|n}(i,j)}{\sum_t \boldsymbol{\pi}_{t-1|n}(i)}, \qquad \hat{\pi}_i = \boldsymbol{\pi}_{1|n}(i), \tag{40}$$

where $\boldsymbol{\pi}_{t|n}(i)$ and $\boldsymbol{\pi}_{t-1,t|n}(i,j)$ are the smoothed marginal and joint probabilities, computed by the standard backward recursion of Hamilton (1989).

D Closed-form yield curve in the two-factor model

Consider the two-factor real-rate model under the risk-neutral measure $\mathbb{Q}$:

$$\begin{cases} dr_t = \kappa^{(r)}(l_t - r_t)\, dt + \sigma^{(r)}\, dW^{(r)}_t, \\ dl_t = \kappa^{(l)}(\nu^{(r)}_t - l_t)\, dt + \sigma^{(l)}\, dW^{(l)}_t, \end{cases} \tag{41}$$

with $d\langle W^{(r)}, W^{(l)}\rangle_t = \rho\, dt$ and risk-neutral long-run mean $\nu^{(r)}_t = \mu^{(r)}_{t,\Delta} - \lambda^{(l)}\sigma^{(l)}/\kappa^{(l)}$, where $\lambda^{(l)}$ is the market price of risk of the long-rate factor calibrated to historical yield-curve levels.

Under $\mathbb{Q}$, the zero-coupon bond price at horizon $\tau = T - t$ is

$$P(t,T) = \exp\bigl[A(\tau) - B_r(\tau)\, r_t - B_l(\tau)\, l_t\bigr], \tag{42}$$

with

$$B_r(\tau) = \Psi(\kappa^{(r)},\tau), \qquad B_l(\tau) = \frac{\kappa^{(r)}}{\kappa^{(r)} - \kappa^{(l)}}\bigl[\Psi(\kappa^{(l)},\tau) - \Psi(\kappa^{(r)},\tau)\bigr], \tag{43}$$

and

$$A(\tau) = -\int_0^\tau \kappa^{(l)}\nu^{(r)}_{t+u} B_l(u)\, du + \int_0^\tau \left[\tfrac{1}{2}(\sigma^{(r)})^2 B_r(u)^2 + \tfrac{1}{2}(\sigma^{(l)})^2 B_l(u)^2 + \rho\sigma^{(r)}\sigma^{(l)} B_r(u) B_l(u)\right] du. \tag{44}$$

When $\nu^{(r)}_{t+u}$ is piecewise constant, with value $\nu^{(r)}_j$ on each interval $[j, j+1)$, the drift integral decomposes as $\int_0^\tau \nu^{(r)}_{t+u} B_l(u)\, du = \sum_j \nu^{(r)}_j \int_j^{\min(j+1,\tau)} B_l(u)\, du$. This is essential in practice since NGFS scenario trajectories are available at annual frequency. Setting $\sigma^{(l)} = 0$ and $l_t = 0$ in (42)–(44) gives the one-factor Hull–White inflation specialization

$$P^{(q)}(t,T) = \exp\left[-\int_0^\tau \kappa^{(q)}\nu^{(q)}_{t+u} B_q(u)\, du + \frac{(\sigma^{(q)})^2}{2}\int_0^\tau B_q(u)^2\, du - B_q(\tau)\, q_t\right],$$

with $B_q(\tau) = \Psi(\kappa^{(q)},\tau)$.

The cross-covariance correction that links real and inflation yields, used in Section 5, has closed form

$$\mathcal{K}(\tau) = \rho_{rq}\sigma^{(r)}\sigma^{(q)}\mathcal{I}(\kappa^{(r)},\kappa^{(q)},\tau) + \rho_{lq}\sigma^{(l)}\sigma^{(q)}\frac{\kappa^{(r)}}{\kappa^{(r)} - \kappa^{(l)}}\bigl[\mathcal{I}(\kappa^{(l)},\kappa^{(q)},\tau) - \mathcal{I}(\kappa^{(r)},\kappa^{(q)},\tau)\bigr], \tag{45}$$

with

$$\mathcal{I}(a,b,\tau) = \frac{1}{ab}\bigl[\tau - \Psi(a,\tau) - \Psi(b,\tau) + \Psi(a+b,\tau)\bigr]. \tag{46}$$

E Asset–liability framework

This appendix collects the mathematical specification of the application in Section 5.

E.1 Bond Book

Under the Gaussian-affine specification, the nominal zero-coupon price factorizes as

$$P^{\text{nom}}(t,t+\tau) = P^{(r)}(t,t+\tau)\, P^{(q)}(t,t+\tau)\, \exp\bigl(\mathcal{K}(\tau)\bigr), \tag{47}$$

with $\mathcal{K}(\tau)$ the cross-covariance correction (45).

Proposition 1 (Nominal yield)**.** *Under the Gaussian-affine specification of Section 3,*

$$y_t^{\mathrm{nom}}(\tau) = y_t^{(r)}(\tau) + y_t^{(q)}(\tau) - \frac{\mathcal{K}(\tau)}{\tau}. \tag{48}$$

Proof. Under $\mathbb{Q}$, the pair $X = -\int_t^{t+\tau} r_u\,du$, $Y = -\int_t^{t+\tau} q_u\,du$ is jointly Gaussian, so $\mathbb{E}^{\mathbb{Q}}[e^{X+Y}] = \mathbb{E}^{\mathbb{Q}}[e^X]\,\mathbb{E}^{\mathbb{Q}}[e^Y]\,\exp(\mathrm{Cov}^{\mathbb{Q}}(X,Y))$ with $\mathrm{Cov}^{\mathbb{Q}}(X,Y) = \mathcal{K}(\tau)$. The simple-rate equivalent yield is $\tilde{y}_t^{\mathrm{nom}}(\tau) = e^{y_t^{\mathrm{nom}}(\tau)} - 1$. □

The bond book is managed to track a target Macaulay duration $\mathcal{T} > 0$. All bonds share a common annual coupon rate $c > 0$; the issuance maturity is selected per cohort. A bond with par N, coupon c, and integer maturity $T \in \mathbb{N}^*$ purchased at t generates the cash-flow stream $\mathrm{CF}_{t+k} = cN$ for $k = 1, \dots, T-1$ and $(1+c)N$ for $k = T$, conditional on no early liquidation. Its MtM at t' with residual maturity $T_{\mathrm{res}} = T - (t' - t)$ is

$$V_{t'}^{\mathrm{bond}}(T_{\mathrm{res}}) = N\left[c\sum_{k=1}^{T_{\mathrm{res}}} P_{t'}^{\mathrm{nom}}(k) + P_{t'}^{\mathrm{nom}}(T_{\mathrm{res}})\right], \tag{49}$$

and its Macaulay duration is the PV-weighted cash-flow date $D_{t'}^{\mathrm{bond}}(T_{\mathrm{res}})$. The aggregate book MtM and book duration are obtained as cohort-weighted sums.

E.2 Annual rebalancing procedure

At each date $t = 1, \dots, H$, the procedure executes nine steps. Matured cohorts are removed from the book, surviving assets are revalued, and bond cash-flows are collected as

$$\mathcal{C}_t = \sum_{T_{\mathrm{res}}>1} cN_{t_0} + \sum_{T_{\mathrm{res}}=1} (1+c)N_{t_0}.$$

The net cash flow is $\Phi_t = \mathcal{C}_t + \xi_t$, with $\Phi_t^- = \max(-\Phi_t, 0)$ and $\Phi_t^+ = \max(\Phi_t, 0)$. If $\Phi_t < 0$, a sequential liquidation waterfall sells equities, then real estate, then bonds, until the deficit is covered. If the total liquidation capacity $\widetilde{V}_t^{(s)} + (1-h)\widetilde{V}_t^{(m)} + \widetilde{V}_t^{\mathrm{bonds}}$ is strictly less than Φ_t^-, the path is declared bankrupt at date t, with $\tau_j(\omega) = t$, $W_t = 0$, $L_t = L_{t-1}(1 + \tilde{q}_t)$, and $K_t = -L_t$.

After the waterfall, the post-waterfall wealth and own-funds levels are

$$W_t^{(6)} = V_t^{(s),\mathrm{adj}} + V_t^{(m),\mathrm{adj}} + V_t^{\mathrm{bonds,adj}} + S_t, \qquad K_t^{(6)} = W_t^{(6)} - L_t,$$

with $S_t = \Phi_t^+$ the residual cash. The triple-target rebalancing then solves for the transaction $(\Delta B, \Delta S, \Delta M)$ that minimizes the quadratic deviation from (16) subject to the cash-balance, HTM, and physical constraints.

Proposition 2 (Triple-target rebalancing)**.** *Let* $\tau_t^M = \gamma\, W_t^{(6)}$ *be the triple-target real-estate position at the post-waterfall wealth level. The optimal real-estate transaction is*

$$\Delta M_t^\star = \begin{cases} \dfrac{V_t^{(m),\mathrm{adj}} - \tau_t^M}{1-\gamma h} \cdot (-1) & \textit{if } V_t^{(m),\mathrm{adj}} > \tau_t^M, \\ \tau_t^M - V_t^{(m),\mathrm{adj}} & \textit{if } V_t^{(m),\mathrm{adj}} \le \tau_t^M, \end{cases} \tag{50}$$

and the final wealth is $W_t^\star = W_t^{(6)} - h\,\Delta M_t^-$, *with* $\Delta M_t^- = \max(-\Delta M_t^\star, 0)$. *The bond and equity transactions are determined by the cash balance and the strategic targets; in the HTM-binding case (when the bond weight exceeds* α_B *at the post-waterfall step),* $\Delta B = 0$ *and the residual cash is allocated to equities.*

NEXIALOG
CONSULTING